Arch Toxicol (2015) 89:243–258
DOI 10.1007/s00204-014-1260-4

MOLECULAR TOXICOLOGY

4-Hydroxy-trans-2-nonenal (4-HNE) induces neuronal SH-SY5Y cell death via hampering ATP binding at kinase domain of Akt1

Mahendra P. Kashyap · Abhishek K. Singh · Dharmendra K. Yadav · Maqsood A. Siddiqui · Ritesh K. Srivastava · Vishal Chaturvedi · Navneet Rai

Received: 13 September 2013 / Accepted: 15 April 2014 / Published online: 14 May 2014

Abstract Inhibition mechanism(s) of protein kinase B/Akt1 and its consequences on related cell signaling were investigated in human neuroblastoma SH-SY5Y cells exposed to 4-hydroxy-trans-2-nonenal (4-HNE), one of the most reactive aldehyde by-products of lipid peroxidation. *In silico* data indicate that 4-HNE interacts with kinase domain of Akt1 with the total docking score of 6.0577 and also forms H-bond to Glu234 residue similar to highly potent Akt1 inhibitor imidazopiperidine analog 8b, in which the protonated imidazole nitrogen involves in two hydrogen bonds between Glu234 and Asp292. The strong hydrogen bonding with Glu234 and hydrophobic interactions with several residues, namely Leu156, Gly157, Val164, Ala177, Tyr229, Ala230, Met281 and Thr291, at the vicinity which is normally occupied by the ribose of ATP, appear to be the main causes of Akt1 inhibition and lead to the significant conformational change on this region of protein. Results of mutational docking prove that Glu234 plays a major role in 4-HNE-mediated Akt1 inhibition. *In silico* data on Akt inhibition were further validated by observing the down-regulated levels of phosphorylated (Thr308/Ser493) Akt1 as well as the altered levels of the downstream targets of pAkt, namely downregulated levels of pGSK3β (Ser9), β-catenin, Bcl_2 and upregulated levels of pro-apoptotic markers, namely Bad, Bax, P^{53} and caspase-9/3. The cellular fate of such pAkt inhibition was evidenced by increased reactive oxygen species, degraded nuclei, transferase dUTP nick end labeling positive cells and upregulated levels of pJNK1/2. We identified that 4-HNE-mediated Akt1 inhibition was due to the competitive inhibition of ATP by 4-HNE at the kinase domain of ATP binding sites.

Keywords Neuronal SH-SY5Y Cells · Akt/Pkb · Apoptosis · 4-HNE · Molecular modeling

Introduction

Peroxidation of ω-6 polyunsaturated fatty acids (PUFA) leads to the generation of various hydroxyalkenals,

M. P. Kashyap (✉) · A. K. Singh
CSIR-Indian Institute of Toxicology Research, Post Box 80, MG Marg, Lucknow 226001, UP, India
e-mail: pratapmkbit@gmail.com; mpk39@pitt.edu

M. P. Kashyap
Department of Urology, University of Pittsburgh School of Medicine, Pittsburgh, PA 15213, USA

A. K. Singh
Department of Biotechnology, Guru Ghasidas Vishwavidyalaya (A Central University), Koni, Bilaspur 495009, Chattisgarh, India

D. K. Yadav
Department of Chemistry, Research Institute for Natural Sciences, Hanyang University, Seoul, Republic of Korea

M. A. Siddiqui
Department of Zoology, College of Science, King Saud University, Riyadh 11451, Saudi Arabia

R. K. Srivastava
Department of Dermatology and Skin Diseases Research Center, University of Alabama at Birmingham, 1530 3rd Avenue South, VH 509, Birmingham, AL 35294-0019, USA

V. Chaturvedi
School of Biomedical Sciences and Curtin Health Innovation Research Institute, Curtin University, Perth, WA 6845, Australia

N. Rai
Genome Centre, University of California, Davis, Davis, CA 95616, USA

including the most abundant lipid peroxidation product, 4-hydroxy-trans-2-nonenal (4-HNE) (Li et al. 2013; Siddiqui et al. 2008b). Up-regulated levels of 4-HNE have been implicated behind the etiology of several neuronal and other disorders including Alzheimer's disease (AD) (Bradley et al. 2010; Butterfield et al. 2010; Li et al. 2013), Parkinson's disease (Wey et al. 2012), ischemia/reperfusion (Hill et al. 2009; Zhang et al. 2005), atherosclerosis (Barski et al. 2013; Leonarduzzi et al. 2005) and obesity/diabetes (Mattson 2009). Radical-mediated peroxidation of unsaturated lipids leads to the generation of reactive alkoyl radicals, which upon spontaneous radical elimination (β-scission) generate several saturated and unsaturated aldehydes (Siddiqui et al. 2008a). The electronegative nature of carbonyl oxygen atom of 4-HNE can initiate the withdrawal of mobile electron density from the β-carbon atom causing regional electron deficiency. On the basis of this type of electron polarizability, 4-HNE is considered a soft electrophile that preferentially form 1,4-Michael-type adducts with soft nucleophiles (LoPachin et al. 2009). 4-HNE has received considerable attention due to its high bio-reactivity and capability to form adducts with cellular nucleophiles such as glutathione, cysteine, lysine and histidine of proteins as well as negative charged nucleic acids (Falletti et al. 2007; Huang et al. 2010; LoPachin et al. 2009).

Accumulated levels of such unsaturated aldehydes and/or their products have been observed under several neuropathological conditions such as (a) increased levels of 4-HNE tissue contents were observed in the diseased regions of brain and spinal fluids of patients suffering from AD and mild cognitive impairment (Srivastava et al. 1998; Williams et al. 2006; Zarkovic 2003); (b) 4-HNE-mediated alkylation in proteins (creatine kinase, tau, neurofilaments and glutamate transporters) has been observed in tissue derived from AD patients (Eliuk et al. 2007; Honzatko et al. 2005; Siddiqui et al. 2008a); (c) positive 4-HNE protein adducts were reported in the cerebral cortex (Lewy bodies, neurons and astrocytes) of patient with dementia and AD (Siddiqui et al. 2008a); (d) 4-HNE-modified proteins were observed in the patients of Parkinson's disease, while high accumulation of 4-HNE was observed in the neurons of Creutzfeldt-Jacob disease (Siddiqui et al. 2008a).

Normally, 4-HNE has 0.1–3.0 μM cellular concentrations, but under oxidative stress, concentration increases ranging from 10 μM to 5 mM (Dianzani 2003). Higher levels of 4-HNE and related aldehydes illicit toxic response, but role of lower levels of 4-HNE cannot be ignored and has already been associated with altered cell signaling (Chaudhary et al. 2013). 4-HNE alters intracellular signaling by activating the oxidative stress, DNA strands break, various MAP kinases, cell cycle arrest and apoptosis pathways. But the mechanism(s) by which 4-HNE inhibits protein kinase B/Akt1, a serine/threonine-specific kinase that plays multiple roles in the regulation of many cellular processes, including cell survival, cell proliferation, apoptosis and glucose metabolism, still remain unclear. Thus, the present investigations were aimed to study the effect of 4-HNE on the inhibition of Akt/protein kinase B and their consequences on downstream cell survival/death signaling pathway(s) in human neuronal SH-SY5Y cells.

Experimental procedures

In silico studies

Molecular modeling parameters and energy minimization

The molecular modeling of compounds, namely Akt inhibitor IV (positive control), 4-HNE (test compound) and SP600125 (negative control), was performed with protein kinase B (Pkb/Akt1) using SYBYL-X 1.3 molecular modeling and drug discovery software (http://www.tripos.com/) [SYBYL-X 1.3, Tripos International, 1699 South Hanley Rd., St. Louis, MO, 63144, USA]. All molecules were initially designed in SYBYL, while the other processes, such as molecular construction, geometry optimization and energy minimization, were performed using HP XW4600 workstation loaded with Intel Core 2 Duo E8400 (3.2 GHz) processor, 4 GB of RAM and Red Hat® Enterprise Linux 4.0 (32-bit compatible) operating system (Silicon Graphics Inc., Mountain View, CA, USA). The Tripos force field with a distance-dependent dielectric and Powell gradient algorithm with a convergence criterion of 0.001 kcal mol^{-1} was used for the optimization. Partial atomic charges were assessed using Gasteiger–Hückel method; 2D structures were converted into 3D structures using the program Concord v4.0, and maximum number of iterations performed in the minimization was set to 2000. Further geometry optimization was done through MOPAC-6 package using the semiempirical PM3 Hamiltonian method (Yadav and Khan 2013).

Molecular docking studies

To explore the possible bioactive conformations of different Akt inhibitors, the SYBYL-X 1.3 interfaced with Surflex-Dock program (Jain 2007) was operated to dock all the compounds into the active site of the Akt kinase (PDB code: 3MV5). This program automatically docks ligand into the binding pocket of an enzyme/receptor

protein, using protomol-based algorithm and empirically produces scoring function. The protomol is very important and necessary factor for docking algorithm and works as a computational representation of proposed ligand that interacts with the binding site. Surflex-Dock's scoring function has several factors which play an important role in the ligand–receptor interaction, in contexts of hydrophobic, polar, repulsive, entropic and solvation. It is a worldwide well-established and recognized method (Pan et al. 2010). Standard docking protocols have ligand flexibility in the docking process and protein counts as a rigid structure (Sander et al. 2008). Our molecular docking process involved several steps including (1) the protein structure was imported into Surflex and hydrogens were added, (2) generation of protomol using a ligand-based strategy. We selected two parameters (first called *protomol_bloat*, which determines how far the site should extend from a potential ligand; and another called *protomol_threshold*, which determines deepness of the atomic probes which used to define the protomol penetration into the protein) to form the appropriate binding pocket. So, in the current study, *protomol_bloat* was set to 0.0, and *protomol_threshold* was set to 0.50, when a reasonable binding pocket was obtained and (3) all of compounds were docked into the binding pocket and 20 possible active docking conformations with different scores were obtained for each compound. During the docking process, all other parameters were assigned their default values. Surflex-Dock total scores, which express the—$\log_{10}$(Kd) units to represent binding affinities, were applied to estimate the ligand–receptor interactions of newly designed molecules.

Mutational docking

Docking simulation-based mutational studies were carried out to further confirm the binding affinity of 4-HNE to these different mutated forms of Akt1. Emphasis was placed on two conserved amino acids. The first one was glutamic acid (Glu234), which was found to be involved in the hydrogen bonding in pre-solved crystal structure of Akt with highly potent Akt inhibitor imidazopiperidine analog (8b) and anilinotriazole analog 5d (Lippa et al. 2008). The other residue was threonine (Thr291), which is also involved in hydrogen bonding with pesticide monocrotophos (Kashyap et al. 2013). Both amino acids were mutated in the ATP binding site of the kinase domain. We changed either Glu234/Thr291 or both Glu234 and Thr291 to find out the importance of these amino acids in the Akt1 inhibition. The Glu234 was replaced with lysine (Lys)/glycine (Gly) or Thr291 was replaced with glycine (Gly) or both Glu234 and Thr291 were replaced with lysine (Lys) and isoleucine (Ile). 4-HNE docking was performed for all the mutants following identical protocol.

In vitro validation studies

Reagents and consumables

All specified chemicals, reagents and diagnostic kits were purchased from Sigma Chemical Company Pvt. Ltd., St. Louis, MO, USA, unless otherwise stated. DMEM/F-12 Ham's culture medium, antibiotics and fetal bovine serum (FBS) were purchased from Gibco BRL, USA. Culture wares and other plastic consumables used in the study were procured from Nunc, USA. Milli Q water (double-distilled deionized water) was used in all experiments. 4-HNE was purchased from Caymen Chemicals, USA, and Akt inhibitor IV was purchased from Millipore, USA.

Cell culture

SH-SY5Y cells were cultured in the following conditions: 5 % CO_2, 95 % atmosphere of high humidity at 37 °C in DMEM/F-12 Ham's cell culture medium supplemented with 10 % FBS, 0.2 % sodium bicarbonate and antibiotic/antimycotic cocktail (1×). For all mechanistic studies, cells at passage 6–15 were used. Viability of the cells was measured by trypan blue dye exclusion, and batches having more than 95 % cell viability were used in the study.

Dose selection of 4-HNE and Akt inhibitor IV

Non-cytotoxic doses of 4-HNE and Akt inhibitor IV used in the present study were identified by standard end point LDH assay using the commercially available LDH assay kit for in vitro cytotoxicity evaluation (TOX-7; Sigma). Briefly, SH-SY5Y cells (1×10^4 cells/well) were seeded in 96-well tissue culture plates and incubated under high humid environment in 5 % CO_2 for 24 h at 37 °C. Culture medium was replaced with fresh DMEM/F12 medium without FBS and supplemented with different concentrations of 4-HNE (1–50 μM) and Akt inhibitor IV (0.1–20 μM). After the respective exposure period (1–12 h), cells were removed from the CO_2 incubator and centrifuged at 250×*g* for 4 min. Then, supernatant from each well was transferred to a fresh flat-bottom 96-well culture plate and processed for LDH enzymatic assay following the instructions and guidelines provided with the kit. A non-cytotoxic doses of 4-HNE (10 μM) and Akt inhibitor IV (2 μM) were further used in this study for the assessment of alterations in the expression of markers of apoptosis and cell death.

Bis-benzimide staining

4-HNE-induced apoptotic alterations were also observed by counting the events of nuclear condensation. Nuclear condensation was observed under fluorescence microscope

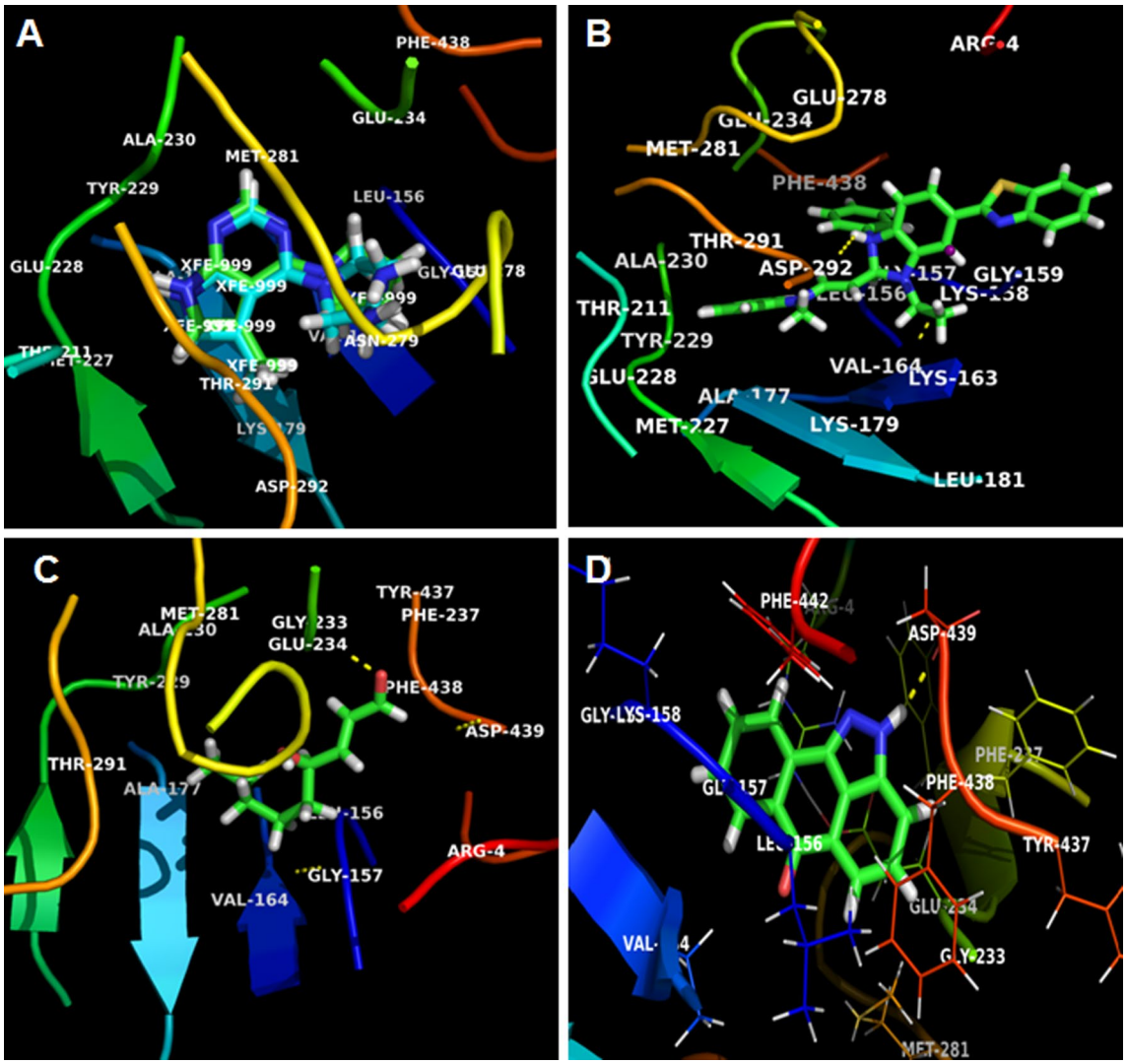

Fig. 1 *In Silico* molecular docking studies elucidating the possible mechanism(s) of 4-hydroxy-trans-2-nonenal (4-HNE)-induced modulation of cell survival protein kinase B (Pkb/Akt). The docking studies were carried out using SYBYL-X 1.3 (Tripos International, 1699 South Hanley Rd., St. Louis, MO, 63144, USA). Protein structure minimization was performed by applying Tripos force field and partial atomic charges were calculated by Gasteiger–Hückel method. Energy minimization was done until the energy change was less than 0.001 kcal/mol. In reasonable binding pocket, all the compounds were docked into the binding pocket, and 20 possible active docking conformations with different scores were obtained for each compound. During the docking process, all of the other parameters were assigned their default values. In complex *red, green, yellow, white* and *purple color* are representing oxygen, carbon, sulfur, hydrogen and nitrogen atoms in ligand–protein complex in docking. **a** The co-crystallized 3-aminopyrrolidine inhibitor was re-docked into the binding site of Akt kinase (PDB: 3MV5) with 0.6381 Å of RMSD between docked and crystallized conformation and total docking score of 6.6819. **b** Akt inhibitor IV docked on to Akt kinase (PDB: 3MV5) with high binding affinity, as indicated by total docking scores of 5.7543. **c** 4-HNE docked on to Akt1 (PDB: 3MV5) with high binding affinity, as indicated by total docking score of 6.0577 comparable to Akt inhibitor IV (positive control). **d** SP600125 (negative control) docked on to Akt1 (PDB: 3MV5) with very low binding affinity, as indicated by total docking score of 3.1147 Akt IV inhibitor (color figure online)

using (2′-[4-ethoxyphenyl]-5-[4-methyl-1-piperazinyl]-2,5′-bi-1H-benzimidazole] (Hochest no. 33342, Sigma, USA) dye as described earlier (Srivastava et al. 2011).

ROS analysis

4-HNE-mediated ROS generation in SH-SY5Y cells was assessed by DCFH-DA dye. In brief, cells (5×10^4 per well) were either seeded in 6-well plates or in 8-well chamber slides and exposed to incomplete DMEM/F-12 Ham's medium containing either 4-HNE (10 μM) or Akt inhibitor IV (2 μM) for 6 h. Following respective exposures, cells were washed twice with PBS and further incubated for 30 min in the dark in incomplete culture medium containing DCFH-DA (20 μM). After washing twice with PBS, cells were analyzed for ROS generation either using

Table 1 Comparison of docking scores and binding site residues of studied compounds against the target Akt1 kinase (PDB: 3MV5)

S. no	Compound	Total energy	Binding pocket residue in (4 Å)	Involved group of amino acid	Length of H-bond Å	No. of hydrogen bond
1.	Akt inhibitor IV (positive) control)	5.7543	ARG-4, LEU-156, GLY-157, GLY-159, PHE-161, LYS-163, VAL-164, ALA-177, LEU-181, THR-211, MET-227, GLU-228, TYR-229, ALA-230, GLU-234, LYS-276, GLU-278, ASN-279, MET-281, THR-291, ASP-292, PHE-438	ASP-230	2.6	1
2.	HNE	6.0577	ARG-4, LEU-156, GLY-157, VAL-164, ALA-177, TYR-229, ALA-230, GLY-233, GLU-234, PHE-237, MET-281, THR-291, TYR-437, ASP-439	GLU-234	1.92	1
3.	SP600125 (negative control)	3.1147	ARG-4, LEU-156, GLY-157, LYS-158, GLY-159, VAL-164, GLY-233, GLU-234, PHE-237, MET-281, TYR-437, PHE-438, ASP-439, PHE-442	ASP-439	1.9	1

Surflex-Dock scores (total scores) were expressed in—log10 (Kd) units to represent binding affinities

fluorescent microscope (Nikon Eclipse 80i equipped with Nikon DS-Ri1 12.7-megapixel camera) or using flow cytometer (BD-LSRSII).

TUNEL assay

Apoptosis was detected by deoxynucleotide transferase dUTP nick end labeling (TUNEL) assays using APO-BrdU TUNEL Assay Kit with Alexa Fluor 488 anti-BrdU (Molecular Probes, Invitrogen Detection Technologies, USA, Catalog No. A23210). We used flow cytometer (BD-FACS Canto, USA) equipped with BD FACS Diva, version 6.1.2 software. Debris was excluded by forward and side-way light-scattering.

Translational studies

Cells were exposed to either 4-HNE (10 μM) or Akt inhibitor IV (2 μM) for 6 h. Altered expression levels of phosphorylated Akt1 (to confirm the *in silico* data of Akt1 inhibition) as well as downstream marker proteins involved in apoptosis and cell death pathways were studied in both experimental and control groups. Proteins harvested from experimental and control groups were processed for Western blot analysis following the protocol described earlier (Kashyap et al. 2010, 2011, 2013). Briefly, 4-HNE-exposed and unexposed cells were pelleted and lysed using Cel-Lytic™ Cell Lysis Reagent (Catalog No. C2978, Sigma, USA) in the presence of 1X protein inhibitor cocktail (Catalog No. P8340, Sigma, USA), 2 mM PMSF and 1 mM sodium orthovanadate. After protein estimation by BCA protein assay (Catalog No. G1002, Lamda Biotech, Inc., St. Louis, MO, USA), equal amounts (20 μg/well) of proteins were loaded in 10–12 % Tricine–SDS gel and blotted on polyvinylidene fluoride (PVDF) membrane using wet transfer system. After blocking for 2 h at 37 °C, the membranes were incubated overnight at 4 °C with specific anti-protein primary antibodies of pGSK3β (Ser9), β-catenin, pAkt (Thr308) and pAkt (Ser473) (1:500), pJNK (1:1,000); p53 (1:500), c-Jun (1:1,000), Bax (1:500), activated caspase-9 and 3 (1:500 and 1:1,000), and β-actin (1:3,000) (CST, USA; Chemicon Inc, USA; BD Biosciences, USA; Santa Cruz, USA) for overnight at 4 °C in blocking buffer (pH 7.5). After several washings, the membranes were then re-incubated with secondary anti-primary immunoglobulin G (IgG) conjugated with horseradish peroxidase (Calbiochem, USA) for 2 h at room temperature. The blots were developed using luminal (Catalog No. 34080, Thermo Scientific, USA) and densitometry for protein specific bands was done in Gel Documentation System (Alpha Innotech, USA) with the help of AlphaEaseTM FC Stand Alone V. 4.0.0 software. β-Actin was used as internal control to normalize the data. 4-HNE-induced alterations in

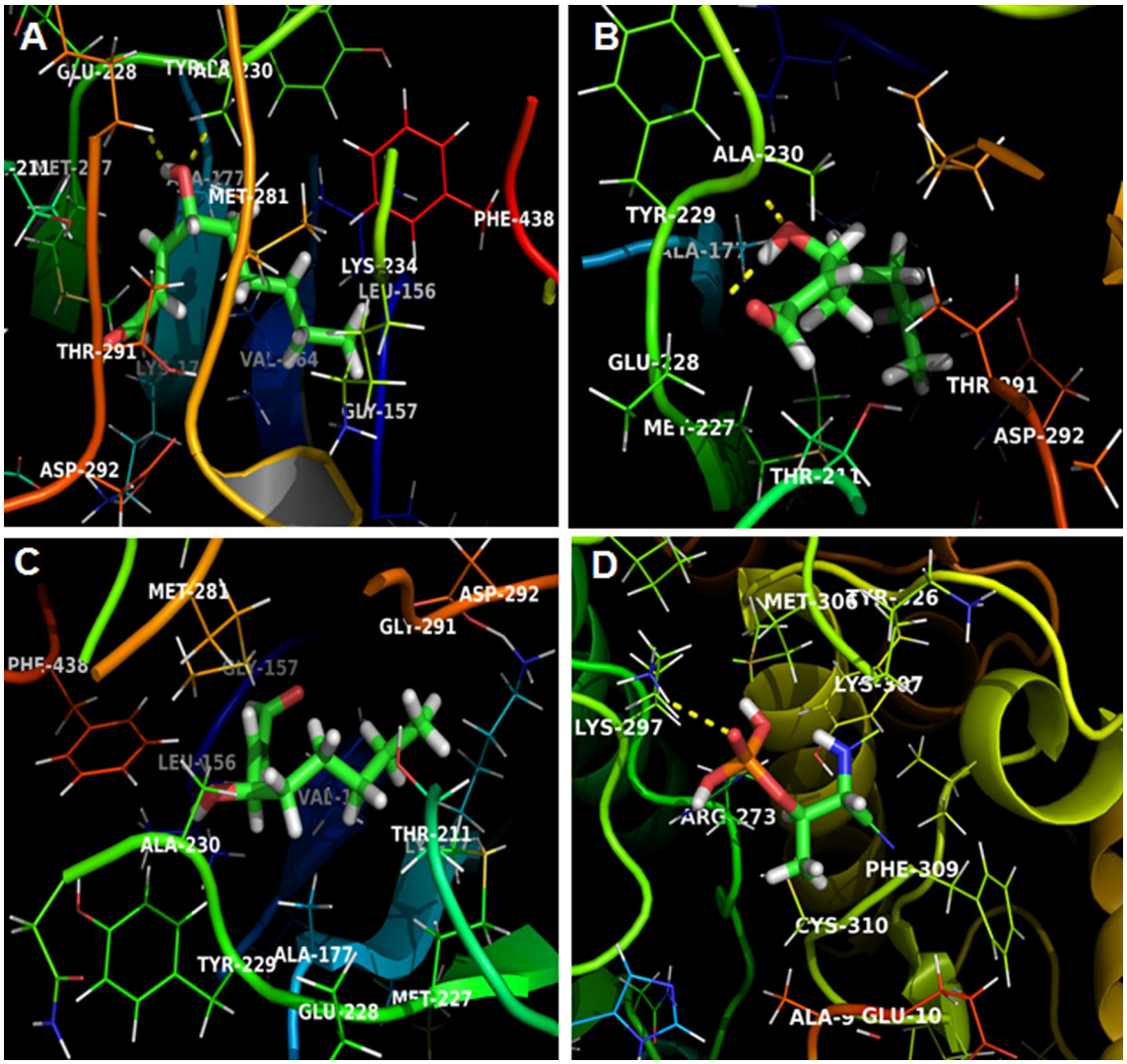

Fig. 2 Mutational docking performed by **a** Glu234 replaced with Lys234 **b** Glu234 replaced with Gly234 **c** Thr291 replaced with Gly291 **d** Glu234 and Thr291 replaced with Lys234 and Ile291 amino acids. In complex *red, green, yellow, white* and *purple color* are representing oxygen, carbon, sulfur, hydrogen and nitrogen atoms in ligand–protein complex in docking (color figure online)

the expression of marker proteins were expressed in fold change compared to relevant unexposed control groups.

Immunocytochemistry

Immunocytochemical localization of anti-apoptotic Bcl_2 was carried out as previously described by us (Kashyap et al. 2011). Briefly, cells (5×10^4 cells/well) were plated in 8-well chamber slides. Cells were exposed to 4-HNE (10 μM) for 6 and 12 h. Following exposure, cells were fixed using 4 % paraformaldehyde for 10 min and blocked with PBS containing 0.3 % Triton X-100 and 5 % BSA for 2 h to block the non-specific binding sites. Cells were then incubated with primary antibody specific to Bcl_2 (1:50, Santa Cruz, USA) for 2 h at room temperature followed by washing with PBS. Cells were further re-incubated with PE-conjugated goat anti-rabbit secondary antibody (1:200, Santa Cruz, USA) for 2 h at room temperature. Finally, cells were washed with PBS to remove any unbound antibody, and then fixed with DAPI containing Fluoromount medium. Cells were visualized under upright fluorescent microscope (Nikon Eclipse 80i equipped with Nikon DS-Ri1 12.7-megapixel camera, Japan).

Statistical analysis

Results were expressed as mean ± standard error of mean (SEM) for the values obtained from at least three independent experiments. Statistical analysis was performed using one-way analysis of variance (ANOVA) and post

Table 2 Comparison of mutational docking scores and binding site residues of studied compounds against the survival target Akt kinase (PDB: 3MV5)

S. no	Compound	Total energy	Biding pocket residue in (4 Å)	Involved group of amino acid	Length of H-bond Å	No. of Hydrogen bond
1.	HNE[a]	3.7014	LEU-156, GLY-157, VAL-164, ALA-177, LYS-179, THR-211, MET-227, GLU-228, TYR-229, ALA-230, LYS-234, MET-281, THR-291, ASP-292, PHE-438	GLU-228 ALA-230	1.8 1.9	2
2.	HNE[b]	3.0092	LEU-156, GLY-157, VAL-164, ALA-177, LYS-179, THR-211, MET-227, GLU-228, TYR-229, ALA-230, MET-281, LYS-289, THR-291, ASP-292, PHE-438	GLU-228 ALA-230	2.0 1.7	2
3.	HNE[c]	5.1896	LEU-156, GLY-157, VAL-164, ALA-177, LYS-179, MET-227, GLU-228, TYR-229, ALA-230, MET-281, GLY-291, ASP-292, PHE-438	–	–	–
4.	HNE[d]	3.0095	TYR-326, MET-306, LYS-297, ARG-273, LYS-307, PHE-309, CYS-310, ALA-9, GLU-10	LYS-297	2.5	1

[a] Glu234 replaced with Lys234

[b] Glu234 replaced with Gly234

[c] Thr291 replaced with Gly291

[d] Glu234 and Thr291 replaced with Lys234 and Ile291 amino acids

hoc Dunnett's (two-sided) test to compare the findings in different groups. The values $P < 0.05$ were considered significant.

Results

In silico molecular docking analysis of 4-HNE with Akt1

The aim of current molecular docking study was to elucidate 4-HNE-mediated conformational changes in the cell survival Akt1/protein kinase B, as well as to study the possible mechanism(s) of action. The results of the molecular docking suggest that studied compounds bind strongly with the kinase domain of Akt1 at a region which also serves as ATP binding pocket. In present investigation, we explored the orientation and binding affinity (in terms of the total score in $-\log_{10}$Kd units to represent binding affinities) of Akt inhibitor IV and 4-HNE toward anti-cancer/cell survival target Akt kinase (PDB code: 3MV5). The docking reliability was validated using the known crystallized X-ray structure of Akt kinase complexes with 3-aminopyrrolidine inhibitor. The co-crystallized 3-aminopyrrolidine inhibitor was re-docked into the binding site, and the docked conformation with the highest total score of 6.6819 was selected as the most probable binding conformation. The low root mean square deviation (RMSD) of 0.6381 Å between the docked and the crystal conformation indicates the high reliability of Surflex-Dock software in reproducing the experimentally observed binding mode for this inhibitor. As shown in Fig. 1, re-docked molecules were almost in the similar position with co-crystallized molecules as at the active site of 3-aminopyrrolidine inhibitor (Fig. 1a).

On the other hand, docking results of positive control, Akt inhibitor IV against anti-cancer/survival target protein Akt kinase, showed high binding affinity indicated by high total score of 5.7543 and formation of a H-bond of length 2.6 Å to the acidic, polar, negative charged residue, i.e., Asp230. In docking of the inhibitor–Akt complex, the chemical nature of binding site residues within a radius of 4 Å were basic (polar, hydrophobic and positive charged), e.g., Arg4 (arginine), Lys163 and 276 (lysine); aromatic (hydrophobic), e.g., Phe161, Phe438 (phenylalanine); Tyr229 (tyrosine); acidic (polar, negative charged), e.g., Glu228, Glu234 and 278 (glutamic acid); Asp292 (aspartic acid); polar amide-type, e.g., Asn279 (asparagine); hydrophobic, e.g., Ala177, Ala230 (alanine); Gly157 and 159 (glycine); Leu156 and 181 (leucine); Met227, Met281 (methionine); and nucleophilic (polar, hydrophobic), e.g., Thr211, Thr291 (threonine); therefore, bound compound showed strong hydrophobic interaction with Akt kinase, which leads to more stability and activity in this compound (Fig. 1b).

Binding affinity obtained in the docking study allowed the activity of the 4-HNE to be compared to that of the standard positive control Akt inhibitor IV. 4-HNE showed

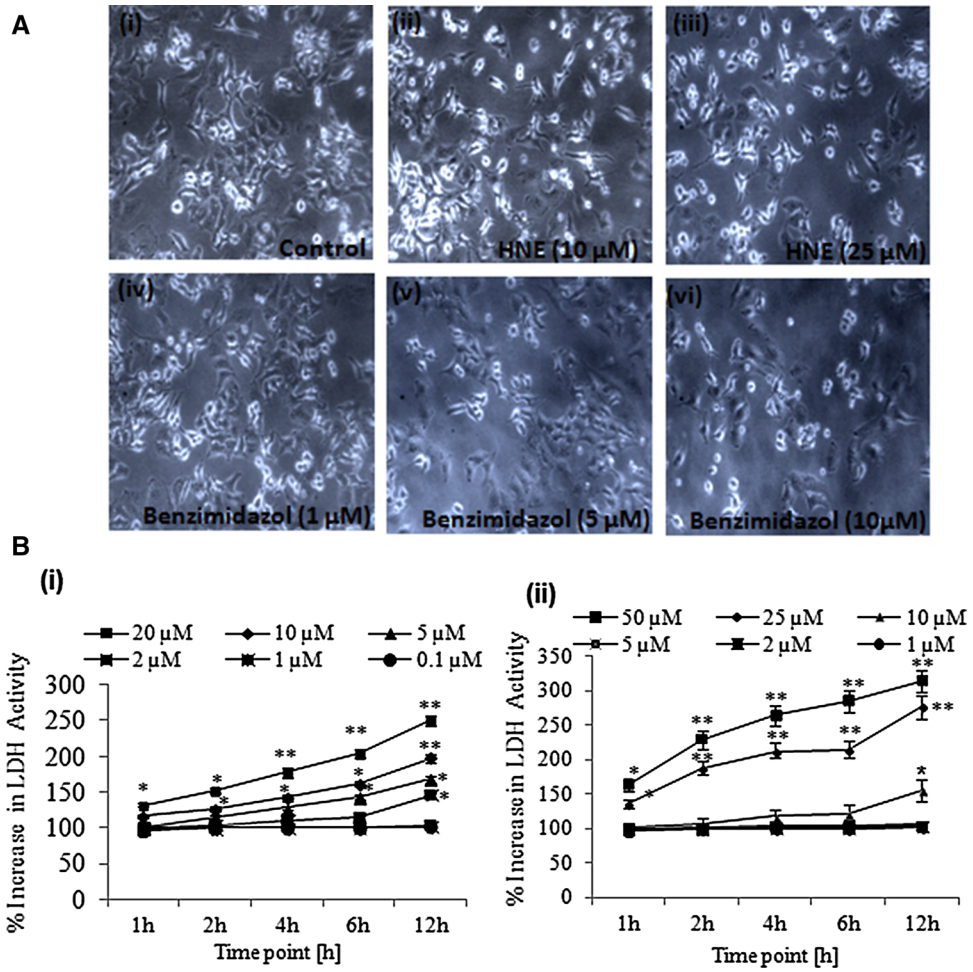

Fig. 3 Cytotoxicity studies: **a** Morphological analysis: unexposed control population (*i*); cells exposed to 10 and 25 μM 4-HNE (*ii* and *iii*) for 6 h; cells exposed to 1, 5 and 10 μM Akt inhibitor IV for 6 h (*iv*, *v*, *vi*). **b** Cytotoxicity studies of Akt inhibitor IV (*i*); 4-HNE (*ii*) by LDH assay

high binding affinity against Akt kinase target protein compared to Akt inhibitor IV with low H-bond length. Upon comparison among the amino acid residues in binding pockets of target protein interacted with test compound, we found that 4-HNE showed molecular interaction with conserved hydrophobic amino acid residues, thus lead to more stability and potency (Table 1). The docking results for 4-HNE showed that the compound docked on anti-cancer target Akt kinase with high binding affinity with docking score indicated by its total score of 6.0577 and also showed the formation of a H-bond of length 1.92 Å to the acidic (polar, negative charged) residue glutamic acid, i.e., Glu234. The 4-HNE–Akt-docked complex also showed similar type of binding site residues within a radius of 4 Å of bound ligand such as basic (polar, hydrophobic and positive charged) residues, e.g., Arg4 (arginine), hydrophobic Leu156 (leucine), hydrophobic, e.g., Ala177, Ala230 (alanine), Gly157 and 233 (glycine); aromatic (hydrophobic) residues, e.g., Phe439, (phenylalanine), Tyr229 and 437 (tyrosine); acidic (polar, negative charged) residues, e.g., Glu234 (glutamic acid), Asp439 (aspartic acid); polar amide-type residue, e.g., hydrophobic residue, e.g., Met281 (methionine); and nucleophilic (polar, hydrophobic) residue, e.g., Thr291 (threonine) when compared to Akt inhibitor IV; therefore, docked molecule also showed strong hydrophobic interaction with Akt kinase, leading to more stability (Fig. 1c).

Docking results for the negative control molecule SP600125 (JNK inhibitor) with Akt kinase showed a low binding affinity, indicated by a low total score of 3.1147 and formation of H-bond, away from ATP binding sites of kinase domain of Akt1 (Fig. 1d). Overall the docking score of 4-HNE was comparable with the known Akt inhibitors such as 3-aminopyrrolidine and Akt inhibitor IV which showed total score of 6.6818 and 5.7543, respectively (Table 1). Thus, docking procedure of Surflex-Dock software (SYBYL-X 1.3) in reproducing the experimental binding affinity seems reliable, so predicted true positive.

Docking studies of 4-HNE with mutational Akt1

Results of mutational docking are summarized in Fig. 2a–d. Briefly, the substitution of negatively charged Glu234 residue (PDB: 3MV5) with positively charged lysine

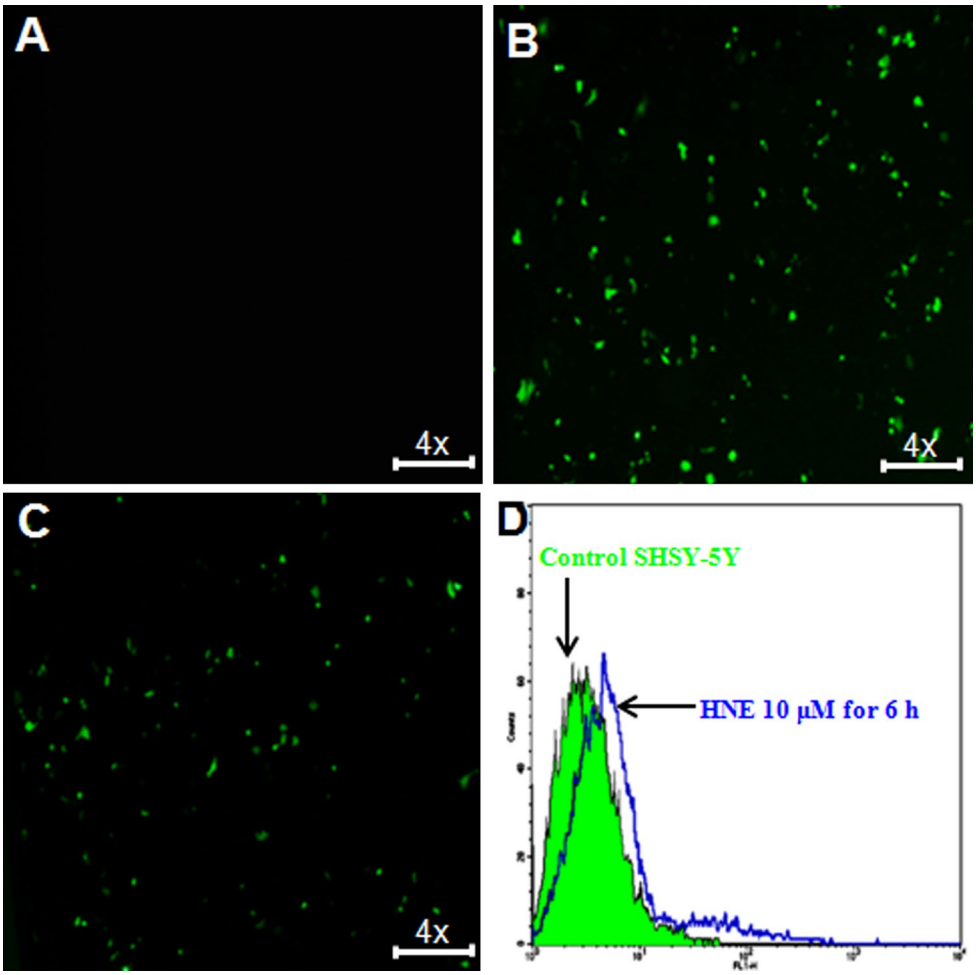

Fig. 4 Representative micro-photographs showing 4-HNE-induced reactive oxygen species (ROS) generation in SH-SY5Y cells. ROS generation was studied using dichlorofluorescin diacetate (DCFH-DA) dye. Images were acquired by Nikon phase contrast cum fluorescence microscope (model 80i). **a** Control SH-SY5Y cells; **b** 4-HNE 10 μM for 6 h; **c** Akt inhibitor IV 2.0 μM for 6 h, **d** change in ROS observed by FACS after exposing SH-SY5Y with 4-HNE 10 μM for 6 h

(Lys) or neutral glycine (Gly) led to huge conformational changes in the structure of this portion of protein. The new mutated Akt–4-HNE complexes have two hydrogen bonds with Glu228 and Ala230 but total energies were decreased by 3.7014 and 3.0092, respectively. Modification at another important residue Thr291 with Gly was lead to small change in energy which decreased to 5.1896 from 6.0577. Simultaneous modifications on both residues Glu234 with Lys, and Thr291 with Ile, further resulted in decrease of the total energy to 3.0095 (Table 2).

In vitro validation studies

Cytotoxicity studies

Prior to using in the experiments, biologically safe doses of 4-HNE and Akt inhibitor IV were identified using lactate dehydrogenase (LDH) release assays. In LDH assay, no significant cytotoxic response was recorded for Akt inhibitor IV (0.1–2 μM) for any time points used in the study except 12 h, while doses 5–20 μM demonstrated time- and concentration-dependent toxicity except 5 μM until 4 h (Fig. 3bi). In case of 4-HNE, no cytotoxicity were observed within 12 h of exposure for 4-HNE concentration lower than 5. At 10 μM, cytotoxicity was observed only at 12 h. Larger 4-HNE concentrations were cytotoxic at all time investigation. In general, 4-HNE (10 μM) exposure for 6 h was found as safe dose in SH-SY5Y cells (Fig. 3bii). Based on these outcomes, further experiments were carried out using a safe dose of 4-HNE (10 μM) for 6 h for protein expression and apoptosis studies. Overall LDH data were well correlated with morphological studies which also exhibited similar trends of cell damage (Fig. 3a(i–vi)).

Induction of ROS generation and bis-benzimide staining

Significant increase in ROS was observed using DCFH-DA dye in cells exposed to 10 μM of 4-HNE and 2 μM Akt inhibitor IV, respectively (Fig. 4a–d). ROS data were well correlated with bis-benzimide data. Apoptosis were significantly increased in cells exposed to 10 μM (14 ± 2 %) and 20 μM (31.66 ± 2.5 %) of 4-HNE compare to unexposed cells (4.66 ± 0.57 %). Moreover, Akt inhibitor IV (2 μM) induced 24 ± 2 % apoptosis in SH-SY5Y cells (Fig. 5a–d).

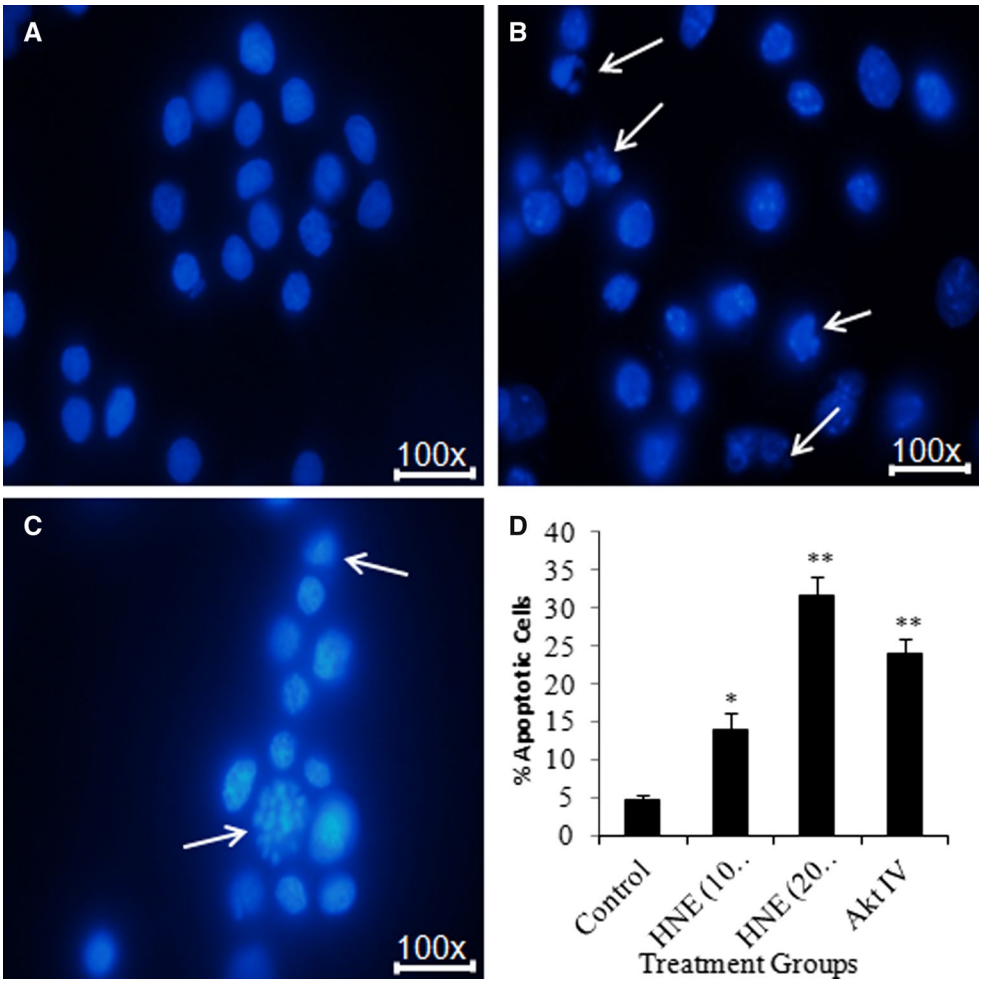

Fig. 5 Apoptosis studies: representative microphotographs of nuclear condensation and nuclear budding as the events to induce apoptosis-mediated cell death assessed by bis-benzimide staining in SH-SY5Y cells exposed to 4-HNE and Akt inhibitor IV. **a** Control SH-SY5Y cells-; **b** cells exposed to 4-HNE 10 μM for 6 h. *Arrows* are showing micronuclei, degenerated nuclei and fragmented apoptotic nuclei; **c** cells exposed to Akt inhibitor IV 2.0 μM for 6 h. *Arrow* is showing babbled fragmented apoptotic nuclei; **d** percentage of apoptotic nuclei/1,000 cells after the exposure to 4-HNE and Akt inhibitor IV. $*P < 0.05$, $**P < 0.001$

TUNEL assay

Our results from deoxynucleotide TUNEL assays also indicated that 4-HNE (10 μM) exposure for 6 h induced significant apoptosis in exposed population (11.14 ± 4.59 %) compared to unexposed cells (4.1 ± 1.93 %). Cells exposed to Akt inhibitor IV (2 μM) for 6 h also demonstrated the significant percentage of apoptosis (13.15 ± 4.47 %) (Fig. 6a–e).

Translational changes

Results of Western blot analysis of 4-HNE (10 μM for 6 h) induced significant changes in the expression of markers involved in Akt/GSK3β/β-catenin and apoptosis pathways in SH-SY5Y are summarized in Fig. 7. In general, the levels of pAkt (Thr308/Ser473), pGSK3β (Ser9) and β-catenin were brought down to 0.62 ± 0.07-fold, 0.48 ± 0.06-fold, 0.47 ± 0.12, 0.69 ± 0.09-fold, respectively, in 4-HNE-exposed SH-SY5Y (Fig. 7a). The magnitude of alterations was also similar for AKT inhibitor IV, positive control used in the study. Although both 4-HNE and Akt inhibitor IV induced alterations in the expression of phosphorylated GSK3β (Ser9), but the changes were significantly lower in case of 4-HNE and comparable with docking study. A significant down-regulation in the expression of survival protein β-catenin was also observed in cells exposed to 4-HNE/Akt inhibitor IV. 4-HNE significantly up-regulate apoptosis markers, namely pJNK1/2 (5.65 ± 0.78-fold/1.81 ± .24-fold), c-JUN (2.44 ± 0.56-fold), BAD (1.59 ± 0.23-fold), P^{53} (1.79 ± 0.23-fold), Bax (2.47 ± 0.34-fold) and activated caspase-9 (3.78 ± 1.2-fold) in SH-SY5Y cells exposed to 4-HNE (Fig. 7b, c). Data of cleaved caspase-3 showed the up-regulation in the level of caspase-3 (1.90 ± 0.34-fold) as well as cleaved caspase-3 (12.61 ± 2.8-fold) in 4-HNE-exposed neuronal SH-SY5Y cells (Fig. 7d).

Immunocytochemical analysis

4-HNE significantly down-regulated the expression of anti-apoptotic protein in time-dependent manner in SH-SY5Y cells. Positive control Akt inhibitor was not the exception of this and posed similar effect on anti-apoptotic Bcl_2 in neuroblastoma cells (Fig. 8).

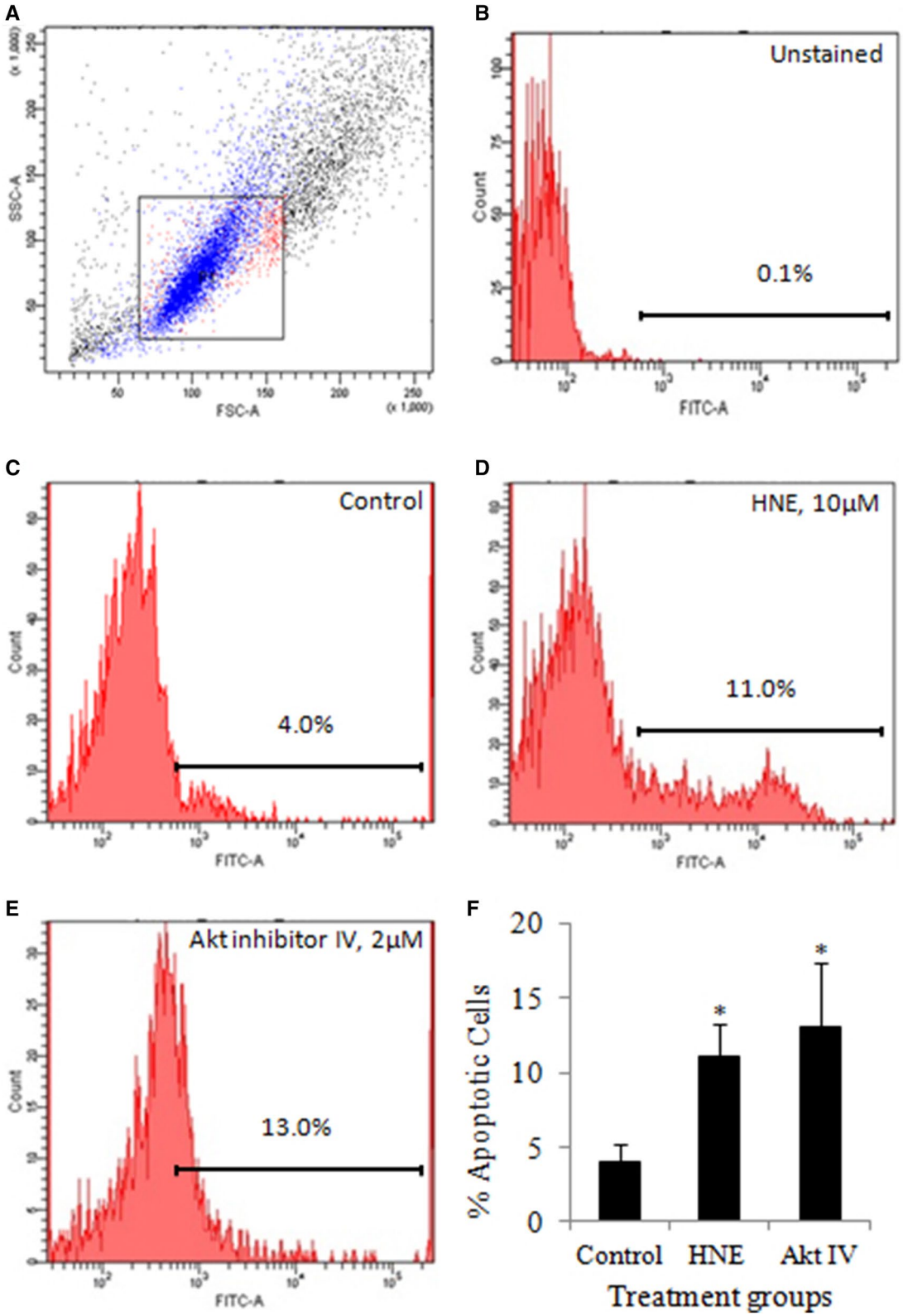

Fig. 6 Validation studies for TUNEL assay were carried out in SH-SY5Y cells by the APO-BrdU TUNEL Assay Kit using cytometer (BD-FACS Canto, USA) equipped with BD FACS Diva, version 6.1.2 software. **a** Gating of the desired population of SH-SY5Y cells; **b** unstained SH-SY5Y cells; **c** control SH-SY5Y cells; **d** cells exposed with 4-HNE 10 μM for 6 h; **e** Akt inhibitor IV 2.0 μM for 6 h; **f** graphical representation of early apoptosis induction in cultured SH-SY5Y cells exposed to 4-HNE 10 μM and Akt inhibitor IV 2.0 μM. $^{*}P < 0.05$, $^{**}P < 0.001$

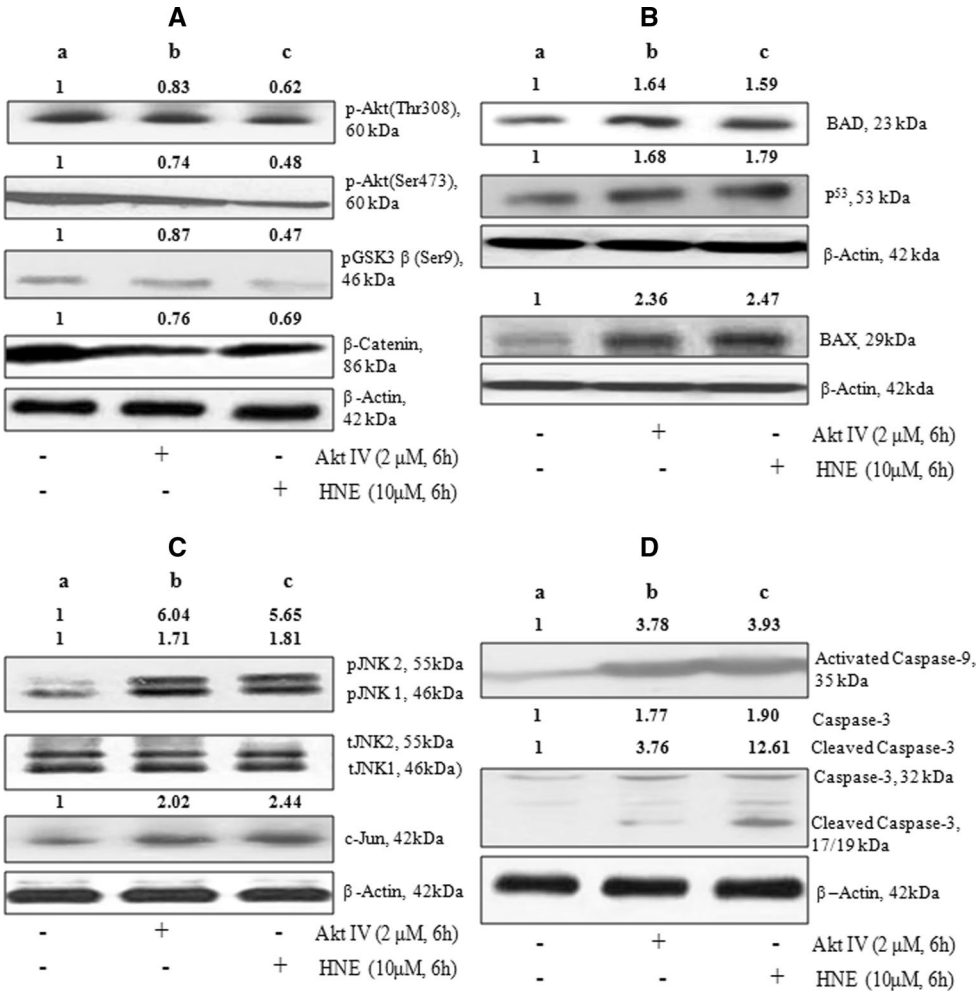

Fig. 7 Western blot analysis to study the translational changes in the selected markers involved in Akt/GSK3b/β-catenin signaling and apoptosis in cultured neuroblastoma SH-SY5Y cells exposed to 4-HNE (10 μM) for 6 h. The data were compared with positive (Akt inhibitor IV) and control (unexposed SH-SY5Y cells). *Lane A* unexposed control cells; *Lane B*: 4-HNE-exposed cells; *Lane C*: cells exposed to AKT inhibitor IV. **a** Analysis of 4-HNE-induced alterations in protein expression of pAkt (Thr308), pAkt (Ser473), pGSK3b (Ser9) and β-catenin. **b** Analysis of 4-HNE-induced alterations in protein expression of MAPKs, namely pJNK1, pJNK2 and c-Jun. **c** Analysis of 4-HNE-induced alterations in protein expression of apoptotic regulators, namely p53; pro-apoptotic markers Bad and Bax. **d** Analysis of 4-HNE-induced alterations in protein expression of activated caspases-9 and 3

Discussion

In our earlier studies, we have reported the metabolism of 4-HNE as well as oxidative stress- and mitochondria-mediated apoptosis in rat pheochromocytoma PC12 cells exposed to 4-HNE (Siddiqui et al. 2008a, 2010a, b, 2012). In the present investigation, we used human SH-SY5Y neuroblastoma cells to investigate the responsiveness of 4-HNE against protein kinase B/Akt1 and its consequences related to survival cell signaling in neuronal SH-SY5Y cells. With the background knowledge that 4-HNE mediates apoptosis with the involvement of p38, MAPK, JNK and concurrent down-regulations of anti-apoptotic Bcl_{xL} and Mcl1 as well as up-regulation of pro-apoptotic Bak (Bodur et al. 2012), we investigated the mechanism of protein kinase B/Akt1 inhibition behind these apoptotic signaling in SH-SY5Y cells. Published studies indicate that 4-HNE exposure causes release of pro-apoptotic Bax from Bcl_2 and phosphorylation of Bcl_2 at Thr56 and Ser70 residues on N-terminal loop which was associated with apoptosis in both U937 and HeLa cells (Bodur et al. 2012).

In the present investigations, human neuroblastoma cells were responded in agreement with other cells exposed to 4-HNE such as PC12 cells (Siddiqui et al. 2008a, b, 2010a, b, 2012), U937 (Bodur et al. 2012) and macrophage cells (Bodur et al. 2012; Haynes et al. 2001). 4-HNE-mediated alterations in the expression of markers associated with oxidative stress, neuronal damage and apoptosis were comparable to our earlier findings with PC12 cells (Siddiqui et al. 2010b). Based on these findings, we hypothesized the involvement of Akt1, also known as protein kinase B (Pkb), in the regulation of whole cascade of 4-HNE-induced apoptosis/cell death. The established role of Akt in the suppression of apoptosis by inhibiting the proteins involved in cell death including ASK1/caspase-9/Bad/P^{53} and P^{21} and promoting the cell survival pathway including IGF-1R/PI3K/PTEN/mTOR (Manning and Cantley 2007) was the key reason behind the current study.

Binding affinities obtained for 4-HNE by docking studies were comparable to standard Akt inhibitor IV. 4-HNE shows high binding affinity against the target protein Akt1 kinase. During the investigation about the interactions of

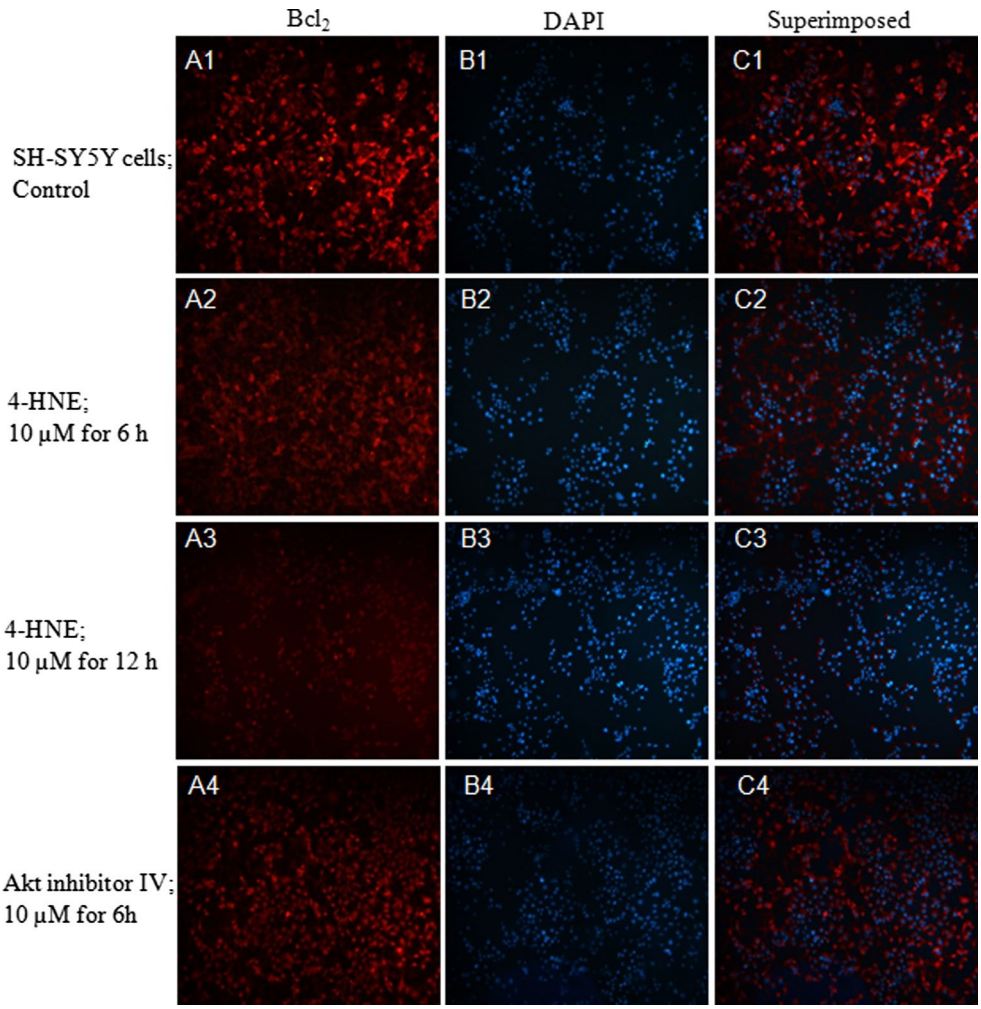

Fig. 8 4-HNE-induced alterations in the expression of anti-apoptotic Bcl_2 protein. Bcl_2 expression was measured using upright phase contrast microscope (Nikon, Japan) at ×10 magnification. *A1* control cells showing intense red color due to high expression of Bcl_2. *A2* and *A3* low *red color* indicates the low expression of Bcl_2 in SH-SY5Y cells exposed to 4-HNE (10 µM) for 6 h and 12 h, respectively. *A4* expression of Bcl2 in cells exposed to Akt inhibitor IV (2 µM) for 6 h. *B1–B4* nuclei stained with DAPI. *C1–C4* superimposed microphotographs showing high expression of Bcl_2 in control in compare to HNE-exposed cells (color figure online)

amino acid residue embedded in binding pocket of Akt1 with the docked 4-HNE, we observed that 4-HNE has molecular interactions with some conserved hydrophobic amino acid residues, which enhanced stability and potency to form 4-HNE–Akt complex. The docking results suggest that 4-HNE has very high binding affinity for Akt1 kinase and also forms H-bond (bond length 1.9 Å) to the acidic, polar, negatively charged residue glutamic acid, i.e., Glu234. For the better understanding of the bindings of 4-HNE to Akt1, we compared our 4-HNE–Akt-docked structure with the pre-solved X-ray co-crystal structure of Akt-imidazopiperidines analog (8b) and anilinotriazole analog 5d (Lippa et al. 2008). Most notably, 4-HNE interacts with Leu156, Gly157, Val164, Ala177, Tyr229, Ala230, Met281 and Thr291 and forms hydrogen bond with Glu234 at the vicinity which was occupied by ribose of ATP (Yang et al. 2002). Similar findings have also been observed in imidazopiperidine analog 8b in which the protonated imidazole nitrogen was involved in two hydrogen bonds with glutamate 234 and aspartate 292 (Lippa et al. 2008). Gurbani et al. (2012) has also reported similar mechanism of inhibition of the ATPase domain of human topoisomerase IIα by different quinone analogs. They demonstrated interactions of quinone analogs, namely 1,4-benzoquinone; 1,2-naphthoquinone; 1,4-naphthoquinone and 9,10-phenanthroquinone with Ser148, Ser149, Asn150 and Asn91 residues of the ATPase domain of Hu-TopoIIα (Gurbani et al. 2012). We also reported similar type of interactions of Akt1 with pesticides monocrotophos, but in the present study, 4-HNE interacts with much higher binding energy even with respect to positive control Akt inhibitor IV (Kashyap et al. 2013). The combined results of the molecular docking and Western blot analysis suggest that 4-HNE significantly inhibits the activity of Akt1 kinase domain by hampering the phosphorylation at position Thr308/Ser473. This might be the result of interactions of 4-HNE at the ATP binding vicinity which finally led competitive inhibition of ATP by 4-HNE at kinase domain of the protein (Kashyap et al. 2013; Lippa et al. 2008). More specifically, our mutational docking data further confirm the importance of H-bond between Glu234 and 4-HNE and seems to have major impact of conformation change

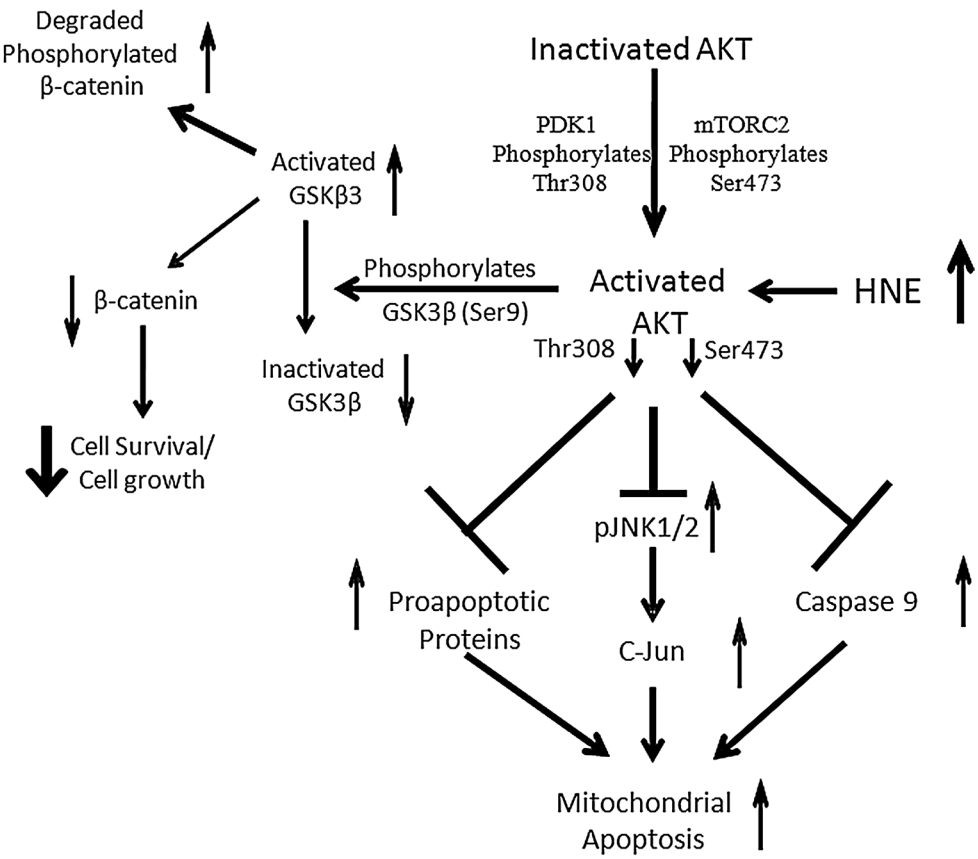

Fig. 9 Schematic flow diagram illustrating the involvement of Akt1 in neuronal cell death by 4-HNE

at kinase domain of Akt1. Although two hydrogen bonds were formed when we replaced Glu234 with either Gly or Lys amino acid in our mutational docking experiments, but still huge loss in the total energy proves the importance of Glu234–HNE interactions at kinase domain. Glu234 usually interacts with ribose of ATP and its strong interaction with 4-HNE resulted unavailability of this site for the ribose of ATP which does not allow the ribose to enter at this region of protein.

Our experimental data revalidate these in silico findings as 4-HNE significantly reduces the phosphorylation of Akt1 at both positions (Thr308 and Ser473). Phosphorylated/activated Akt1 further inactivates the GSK3β by phosphorylating it at Ser9 (Manning and Cantley 2007). In our study, reduced levels of phosphorylated GSK3β (Ser9) and β-catenin suggest degradation of β-catenin through ubiquitin-dependent proteosomal pathway, which leads to apoptosis in the neuronal SH-SY5Y cells. The activation of GSK3β is also known to inhibit the Wnt/frizzled/disheveled (DSH) pathway to promote cell survival and cell growth (Manning and Cantley 2007). Thus, the reduced levels of pAkt, pGSK3β and β-catenin in present investigation suggest impaired Wnt/Akt/GSK3β/β-catenin signaling and subsequent induction of apoptosis in neuroblastoma exposed to 4-HNE.

Protective role of pAkt is reported primarily by NFκB survival signaling, inhibiting ASK1, which eventually blocks the phosphorylation of downstream JNK1/2 (Manning and Cantley 2007). Increased levels of pJNK1/2 have been reported to induce apoptosis via the activation of downstream molecules, namely P^{53}, P^{21}, Bax and caspases in a variety of cells (Galluzzi et al. 2009; Kashyap et al. 2013). In agreement to these earlier findings, present investigation also confirms the up-regulation of pJNK1/2, c-Jun, Bax, activated caspase-9 and caspase-3 in 4-HNE-exposed neuroblastoma cells. Our findings indicate that 4-HNE induced apoptosis via the involvement of the different pathways related to DNA damage and oxidative stress.

Soluble pro-apoptotic protein (Bad) interacts with the anti-apoptotic proteins Bcl_2/Bcl_{xL} into the mitochondrial membrane and prevents the anti-apoptotic activity of these proteins via preventing their interactions with pro-apoptotic Bax (Galluzzi et al. 2009; Manning and Cantley 2007). As a result, Bax creates homo-oligomeric channels in the mitochondrial membrane and leads to the release of cytochrome-*c* from mitochondria to cytoplasm. Cytochrome-*c* interacts with the adapter protein Apaf-1, which leads to caspase-regulated and mitochondrial-mediated cell death (Galluzzi et al. 2009; Kashyap et al. 2010, 2011). There are indirect, but important evidence showing

the effect of Akt signaling on cell survival in the maintenance of mitochondrial membrane potential (Plas and Thompson 2005; Robey and Hay 2006). Thus, significantly increased expression levels of the Bad, Bax, activated caspase 9 and caspase 3 indicate the involvement of mitochondrial proteins in 4-HNE-induced apoptosis and cell injury in SH-SY5Y cells.

In summary, Akt1 plays a key role in the regulation of 4-HNE-induced apoptosis in neuronal SH-SY5Y cells. 4-HNE shows strong binding interactions with the kinase domain of protein kinase B/Akt1 at ATP binding vicinity. These interactions impair the phosphorylation of Pkb/Akt1 at Thr309 and Ser473. 4-HNE-mediated down-regulation of pAkt in SH-SY5Y cells was found to be associated with the impaired expression of pAkt/pGSK3β/β-catenin signaling pathway. At the same time, up-regulated expression levels of pJNK1/2, C-Jun and Bad could be associated with the up-regulated expressions of P^{53}, Bax, activated caspase-9/3 and reduced Bcl_2 (Fig. 9).

Conclusion

Our data demonstrate that Akt1 protein plays a key role in 4-HNE-induced apoptosis in neuronal SH-SY5Y cells. We also identify molecular mechanism that further explains action of 4-HNE through competitive inhibition of ATP at kinase domain of protein kinase B/Akt1. 4-HNE induces the cellular responses through strong binding and inhibition of phosphorylation at kinase domain of Akt1 protein, and its interaction with Glu234 residue at ATP binding site plays a major role behind such inhibition.

Acknowledgments The University Grant Commission (UGC), New Delhi, India, is acknowledged for providing financial support to Dr. Mahendra P. Kashyap. The funders had no role in study design, data collection and analysis, decision to publish or preparation of the article.

Conflict of interest The authors declare that they have no conflict of interest.

References

Barski OA, Xie Z, Baba SP et al (2013) Dietary carnosine prevents early atherosclerotic lesion formation in apolipoprotein E-null mice. Arterioscler Thromb Vasc Biol 33(6):1162–1170. doi:10.1161/ATVBAHA.112.300572

Bodur C, Kutuk O, Tezil T, Basaga H (2012) Inactivation of Bcl-2 through IkappaB kinase (IKK)-dependent phosphorylation mediates apoptosis upon exposure to 4-hydroxynonenal (HNE). J Cell Physiol 227(11):3556–3565. doi:10.1002/jcp.24057

Bradley MA, Markesbery WR, Lovell MA (2010) Increased levels of 4-hydroxynonenal and acrolein in the brain in preclinical Alzheimer disease. Free Radic Biol Med 48(12):1570–1576. doi:10.1016/j.freeradbiomed.2010.02.016

Butterfield DA, Bader Lange ML, Sultana R (2010) Involvements of the lipid peroxidation product, HNE, in the pathogenesis and progression of Alzheimer's disease. Biochim Biophys Acta 1801(8):924–929. doi:10.1016/j.bbalip.2010.02.005

Chaudhary P, Sharma R, Sahu M, Vishwanatha JK, Awasthi S, Awasthi YC (2013) 4-Hydroxynonenal induces G2/M phase cell cycle arrest by activation of the ataxia telangiectasia mutated and Rad3-related protein (ATR)/checkpoint Kinase 1 (Chk1) signaling pathway. J Biol Chem 288(28):20532–20546. doi:10.1074/jbc.M113.467662

Dianzani MU (2003) 4-Hydroxynonenal from pathology to physiology. Mol Aspects Med 24(4–5):263–272

Eliuk SM, Renfrow MB, Shonsey EM, Barnes S, Kim H (2007) Active site modifications of the brain isoform of creatine kinase by 4-hydroxy-2-nonenal correlate with reduced enzyme activity: mapping of modified sites by Fourier transform-ion cyclotron resonance mass spectrometry. Chem Res Toxicol 20(9):1260–1268. doi:10.1021/tx7000948

Falletti O, Cadet J, Favier A, Douki T (2007) Trapping of 4-hydroxynonenal by glutathione efficiently prevents formation of DNA adducts in human cells. Free Radic Biol Med 42(8):1258–1269. doi:10.1016/j.freeradbiomed.2007.01.024

Galluzzi L, Blomgren K, Kroemer G (2009) Mitochondrial membrane permeabilization in neuronal injury. Nat Rev Neurosci 10(7):481–494. doi:10.1038/nrn2665

Gurbani D, Kukshal V, Laubenthal J et al (2012) Mechanism of inhibition of the ATPase domain of human topoisomerase IIalpha by 1,4-benzoquinone, 1,2-naphthoquinone, 1,4-naphthoquinone, and 9,10-phenanthroquinone. Toxicol Sci 126(2):372–390. doi:10.1093/toxsci/kfr345

Haynes RL, Brune B, Townsend AJ (2001) Apoptosis in RAW 264.7 cells exposed to 4-hydroxy-2-nonenal: dependence on cytochrome C release but not p53 accumulation. Free Radic Biol Med 30(8):884–894

Hill BG, Awe SO, Vladykovskaya E et al (2009) Myocardial ischaemia inhibits mitochondrial metabolism of 4-hydroxy-trans-2-nonenal. Biochem J 417(2):513–524. doi:10.1042/BJ20081615

Honzatko A, Brichac J, Murphy TC et al (2005) Enantioselective metabolism of trans-4-hydroxy-2-nonenal by brain mitochondria. Free Radic Biol Med 39(7):913–924. doi:10.1016/j.freeradbiomed.2005.05.010

Huang H, Kozekov ID, Kozekova A et al (2010) DNA cross-link induced by trans-4-hydroxynonenal. Environ Mol Mutagen 51(6):625–634. doi:10.1002/em.20599

Jain AN (2007) Surflex-Dock 2.1: robust performance from ligand energetic modeling, ring flexibility, and knowledge-based search. J Comput Aided Mol Des 21(5):281–306. doi:10.1007/s10822-007-9114-2

Kashyap MP, Singh AK, Siddiqui MA et al (2010) Caspase cascade regulated mitochondria mediated apoptosis in monocrotophos exposed PC12 cells. Chem Res Toxicol 23(11):1663–1672. doi:10.1021/tx100234m

Kashyap MP, Singh AK, Kumar V et al (2011) Monocrotophos induced apoptosis in PC12 cells: role of xenobiotic metabolizing cytochrome P450 s. PLoS ONE 6(3):e17757. doi:10.1371/journal.pone.0017757

Kashyap MP, Singh AK, Kumar V et al (2013) Pkb/Akt1 mediates Wnt/GSK3beta/beta-catenin signaling-induced apoptosis in human cord blood stem cells exposed to organophosphate pesticide monocrotophos. Stem Cells Dev 22(2):224–238. doi:10.1089/scd.2012.0220

Leonarduzzi G, Chiarpotto E, Biasi F, Poli G (2005) 4-Hydroxynonenal and cholesterol oxidation products in atherosclerosis. Mol Nutr Food Res 49(11):1044–1049. doi:10.1002/mnfr.200500090

Li Q, Sadhukhan S, Berthiaume JM et al (2013) 4-Hydroxy-2(E)-nonenal (HNE) catabolism and formation of HNE adducts are

modulated by beta oxidation of fatty acids in the isolated rat heart. Free Radic Biol Med 58:35–44. doi:10.1016/j.freeradbiomed.2013.01.005

Lippa B, Pan G, Corbett M et al (2008) Synthesis and structure based optimization of novel Akt inhibitors. Bioorg Med Chem Lett 18(11):3359–3363. doi:10.1016/j.bmcl.2008.04.034

LoPachin RM, Gavin T, Petersen DR, Barber DS (2009) Molecular mechanisms of 4-hydroxy-2-nonenal and acrolein toxicity: nucleophilic targets and adduct formation. Chem Res Toxicol 22(9):1499–1508. doi:10.1021/tx900147g

Manning BD, Cantley LC (2007) AKT/PKB signaling: navigating downstream. Cell 129(7):1261–1274. doi:10.1016/j.cell.2007.06.009

Mattson MP (2009) Roles of the lipid peroxidation product 4-hydroxynonenal in obesity, the metabolic syndrome, and associated vascular and neurodegenerative disorders. Exp Gerontol 44(10):625–633. doi:10.1016/j.exger.2009.07.003

Pan J, Liu GY, Cheng J, Chen XJ, Ju XL (2010) CoMFA and molecular docking studies of benzoxazoles and benzothiazoles as CYP450 1A1 inhibitors. Eur J Med Chem 45(3):967–972. doi:10.1016/j.ejmech.2009.11.037

Plas DR, Thompson CB (2005) Akt-dependent transformation: there is more to growth than just surviving. Oncogene 24(50):7435–7442. doi:10.1038/sj.onc.1209097

Robey RB, Hay N (2006) Mitochondrial hexokinases, novel mediators of the effects of growth factors and Akt. Oncogene 25(34):4683–4696. doi:10.1038/sj.onc.1209595

Sander T, Liljefors T, Balle T (2008) Prediction of the receptor conformation for iGluR2 agonist binding: QM/MM docking to an extensive conformational ensemble generated using normal mode analysis. J Mol Graph Model 26(8):1259–1268. doi:10.1016/j.jmgm.2007.11.006

Siddiqui MA, Kashyap MP, Khanna VK et al (2008a) Metabolism of 4-hydroxy trans 2-nonenal (HNE) in cultured PC-12 cells. Ann Neurosci 15(3):60–68

Siddiqui MA, Singh G, Kashyap MP et al (2008b) Influence of cytotoxic doses of 4-hydroxynonenal on selected neurotransmitter receptors in PC-12 cells. Toxicol In Vitro 22(7):1681–1688. doi:10.1016/j.tiv.2008.07.001

Siddiqui MA, Kashyap MP, Khanna VK, Yadav S, Pant AB (2010a) NGF induced differentiated PC12 cells as in vitro tool to study 4-hydroxynonenal induced cellular damage. Toxicol In Vitro 24(6):1681–1688. doi:10.1016/j.tiv.2010.05.019

Siddiqui MA, Kashyap MP, Kumar V, Al-Khedhairy AA, Musarrat J, Pant AB (2010b) Protective potential of trans-resveratrol against 4-hydroxynonenal induced damage in PC12 cells. Toxicol In Vitro 24(6):1592–1598. doi:10.1016/j.tiv.2010.06.008

Siddiqui MA, Kumar V, Kashyap MP et al (2012) Short-term exposure of 4-hydroxynonenal induces mitochondria-mediated apoptosis in PC12 cells. Hum Exp Toxicol 31(4):336–345. doi:10.1177/0960327111432500

Srivastava S, Chandra A, Wang LF et al (1998) Metabolism of the lipid peroxidation product, 4-hydroxy-trans-2-nonenal, in isolated perfused rat heart. J Biol Chem 273(18):10893–10900

Srivastava RK, Pant AB, Kashyap MP, Kumar V, Lohani M, Jonas L, Rahman Q (2011) Multi-walled carbon nanotubes induce oxidative stress and apoptosis in human lung cancer cell line-A549. Nanotoxicology 5(2):195–207. doi:10.3109/17435390.2010.503944

Wey MC, Fernandez E, Martinez PA, Sullivan P, Goldstein DS, Strong R (2012) Neurodegeneration and motor dysfunction in mice lacking cytosolic and mitochondrial aldehyde dehydrogenases: implications for Parkinson's disease. PLoS ONE 7(2):e31522. doi:10.1371/journal.pone.0031522

Williams TI, Lynn BC, Markesbery WR, Lovell MA (2006) Increased levels of 4-hydroxynonenal and acrolein, neurotoxic markers of lipid peroxidation, in the brain in mild cognitive impairment and early Alzheimer's disease. Neurobiol Aging 27(8):1094–1099. doi:10.1016/j.neurobiolaging.2005.06.004

Yadav DK, Khan F (2013) QSAR, docking and ADMET studies of camptothecin derivatives as inhibitors of DNA topoisomerase-I. J Chemom 27:21–33

Yang J, Cron P, Good VM, Thompson V, Hemmings BA, Barford D (2002) Crystal structure of an activated Akt/protein kinase B ternary complex with GSK3-peptide and AMP-PNP. Nat Struct Biol 9(12):940–944. doi:10.1038/nsb870

Zarkovic K (2003) 4-Hydroxynonenal and neurodegenerative diseases. Mol Aspects Med 24(4–5):293–303

Zhang N, Komine-Kobayashi M, Tanaka R, Liu M, Mizuno Y, Urabe T (2005) Edaravone reduces early accumulation of oxidative products and sequential inflammatory responses after transient focal ischemia in mice brain. Stroke 36(10):2220–2225. doi:10.1161/01.STR.0000182241.07096.06